Chemical Selectivity in Electrochemical Surface Oxidation Enhanced Raman Scattering.

Martin Perez-Estebanez[1], Sheila Hernandez[1], Juan V. Perales-Rondon[1,2], Elvira Gomez[3], Aranzazu Heras[1], Alvaro Colina[1]*.*

[1] Department of Chemistry, Universidad de Burgos, Pza. Misael Bañuelos s/n, E-09001 Burgos (Spain)

[2] Department of Analytical Chemistry, Physical Chemistry and Chemical Engineering, University of Alcala. Ctra. Madrid-Barcelona, Km. 33.600, 28871 Alcalá de Henares, Madrid, Spain.

[3] Grup d'Electrodeposició de Capes Primes i Nanoestructures (GE-CPN), Dep. Ciència de Materials i Química Física and Institut de Nanociència i Nanotecnologia (IN2UB), Universitat de Barcelona, E-08028, Barcelona (Spain).

* Corresponding author: acolina@ubu.es, jvperales@ubu.es

ABSTRACT

Electrochemical Surface Oxidation Enhancement Raman Scattering (EC-SOERS) is an interesting and promising phenomenon capable of amplifying the Raman signal in a similar way to Surface Enhanced Raman Scattering (SERS), but EC-SOERS takes place during the oxidation of a silver substrate. This phenomenon was originally described for specific electrolytic conditions in which a small amount of chloride in acidic media was mandatory to obtain a substantial enhancement. Herein, we demonstrate that EC-SOERS can be also observed in presence of KBr, showing a potential-dependent behavior. Moreover, in this work a novel approach to reach chemical selectivity during time resolved Raman spectroelectrochemistry (TR-Raman-SEC) experiments is proposed. This new approach is based on the effect of the electrolytic medium on the structures that are formed on the electrode surface. SEM studies were carried out to study the origin of this selectivity. Although SEM images reveal clear differences between the structures of silver halides formed on the electrode surface during the oxidation of the substrate, the absence of EC-SOERS effect at open circuit potential hinders the identification of the actual structures responsible for the phenomenon.

Keywords: Spectroelectrochemistry; Raman; SERS; EC-SOERS; silver roughening.

INTRODUCTION

Raman spectroscopy is a well-known instrumental technique that provides spectroscopic fingerprints of molecules [1,2]. The intrinsic lack of sensitivity of Raman spectroscopy has limited its use for many years in analytical applications. However, when the surface enhanced Raman scattering (SERS) effect was discovered [3], scientific community became more interested in Raman spectroscopy [4–7]. Since then, multiple ways to improve the performance of Raman spectroscopy have been developed [8–16]. Among them, spectroelectrochemical methods are particularly useful, since they allow the generation and the improvement of SERS substrates [7,17–22], as well as the simultaneous measurement of the spectroscopic response. Recently, our research group discovered a new phenomenon related to SERS, but with some significant differences. We observed that, during the electrochemical generation of SERS substrates, the enhancement of the Raman signal can be also observed during the oxidation of a silver substrate. We have called this phenomenon electrochemical surface oxidation enhanced Raman scattering (EC-SOERS), and it has been described for specific electrolytic conditions [23].

SERS is a phenomenon related to the amplification of the Raman signal of molecules located at or really close to metallic nanostructures with plasmonic properties [24,25]. Such Raman enhancement can reach several orders of magnitude and involves two main mechanisms, namely, the electromagnetic [5,17] and the chemical mechanism [4] . Theoretically, the chemical mechanism contributes to an enhancement up to 10^3 for para- and meta-substituted pyridine interacting with silver clusters, but in practice, these increments are usually lower than 10^3 [3,4,26]. Therefore, Raman enhancements higher than 10^3 have to be related to the

so-called electromagnetic mechanism, classically ascribed to the presence of plasmonic nanostructures.

Typically, during subsequent oxidation-reduction cycles (ORC) of a metal electrode such as Cu, Ag or Au, plasmonic nanostructures are formed on the surface[17,27–31]. Thus, when performing an ORC on a metal substrate using TR-Raman-SEC, it is expected that the SERS effect will emerge at cathodic overpotentials, where the reduction of metal ions previously generated by oxidation of the electrode surface and the formation of plasmonic nanostructures take place. Conversely, the loss of the Raman signal due to the SERS effect is expected at anodic overpotentials, due to the oxidation of these nanostructures [23,32].

As was aforementioned, EC-SOERS is an intriguing phenomenon which implies a huge enhancement of the Raman signal during the oxidation stage of a silver electrode [23]. This new phenomenon cannot be easily explained by the classical SERS theory, since the main structures responsible of SERS effect (roughened silver or silver nanoparticles) are superficially destroyed or damaged during oxidation stage, hindering the Raman response. Moreover, typical Raman probe molecules, such as pyridine or cyanide do not present Raman enhancement during this oxidation process [23]. So far, EC-SOERS has only been described in acidic media with specific concentrations of KCl, being the optimal medium to observe this phenomenon 0.1 M $HClO_4$ + $5 \cdot 10^{-3}$ M KCl, and Ag electrodes as substrates [23]. In our last study, both the concentration of KCl and the pH demonstrated to be fundamental to reach a good and reproducible EC-SOERS signal [33]. In this work, we amplify the knowledge about this phenomenon by using different experimental conditions. Here, the effect of the electrolytic medium was studied, changing KCl for KBr and modifying the solution pH. Thus, we will demonstrate for the first time that EC-SOERS can be also observed using bromide instead of

chloride. This fact surprisingly allowed us to detect certain chemical selectivity to some molecules, only by changing the halide solution. Therefore, the optimization of the experimental conditions was performed to achieve this chemical selectivity in EC-SOERS experiments by using different electrolytic media. As a proof of concept, this chemical selectivity is demonstrated with two well-known molecules, uric acid (UA) and benzoic acid (BzA), which exhibit good EC-SOERS responses.

EXPERIMENTAL SECTION

Reagents and solutions

Perchloric acid ($HClO_4$, 60%, Sigma-Aldrich), potassium chloride (KCl, 99%, ACROS Organics), potassium bromide (KBr, 99%, ACROS Organics), uric acid (UA, 99%, ACROS Organics), benzoic acid (BzA, 99.5%, Panreac), salicylic acid (>99%, Sigma-Aldrich), acetylsalicylic acid (AcSa, >99%, Sigma-Aldrich), caffeine (>99%, Sigma-Aldrich), citric acid (99,5%, Panreac), sorbic acid (pure, Probus). All solutions were prepared using ultrapure water obtained from a Millipore DirectQ purification system provided by Millipore (18.2 MΩ·cm resistivity at 25 ºC).

Instrumentation

Time resolved Raman spectroelectrochemistry

In-situ time-resolved Raman spectroelectrochemistry (TR-Raman-SEC) was performed with a customized SPELEC-RAMAN instrument (Metrohm-DropSens), which includes a 785 nm laser source. The laser power in all experiments was set at 80 mW (254 $W \cdot cm^{-2}$). This instrument was connected to a Raman probe (DRP-RAMANPROBE, Metrohm-DropSens). A

homemade cell for screen-printed electrodes or disk electrodes was used during the experiments. DropView SPELEC software (Metrohm-DropSens) was used to control the instrument, which allows getting real-time and synchronized spectroelectrochemical data. An integration time of 1 s was used for all the TR-Raman-SEC experiments. Silver disk electrodes (d=3 mm) were used as working electrodes, a home-made Ag/AgCl (3 M KCl) electrode was used as reference and a platinum wire as auxiliary electrode in certain experiments. Some experiments were carried out using silver screen-printed electrodes (Ag-SPEs, DRP-C013, Metrohm-DropSens) that consist of a silver disc of d=1.6 mm as working electrode, a silver pseudo-reference electrode and a carbon auxiliary electrode. Experiments carried out using Ag-SPEs and bromide electrolytic media were performed using an external home-made Ag/AgCl (3 M KCl) reference electrode.

Scanning electron microscope images

FE-SEM images were obtained using a Field Emission JSM-7100 Analytical Microscope (JEOL Ltd.).

TR-Raman spectroelectrochemistry measurements

Linear sweep voltammetry (LSV) and cyclic voltammetry (CV) were used as electrochemical techniques to perform TR-Raman-SEC experiments. LSV was performed from 0.00 V to +0.60 V, whereas CV were usually performed between -0.25 V and +0.55 V, starting at 0.00 V in the anodic direction. A scan rate of 0.02 V s^{-1} and a step potential of 2 mV were set for all electrochemical measurements. All potentials refer to the Ag/AgCl (3 M KCl) reference electrode.

In order to obtain a reproducible EC-SOERS signal, Ag-SPEs were conditioned before each experiment performing 2 CVs as described above, using the corresponding electrolytic medium without the target analyte. In the experiments carried out with Ag-SPEs using $1 \cdot 10^{-3}$ M $HClO_4$ + $5.4 \cdot 10^{-2}$ M $LiClO_4$ + $5 \cdot 10^{-2}$ M KBr + $1 \cdot 10^{-3}$ M BzA as electrolytic medium, one different pretreatment that consists of two CVs at 0.02 V s^{-1} between -0.60 V and +0.60 V, starting from 0.00 V in the anodic direction was performed, in order to achieve the total reduction of the large amount of AgBr formed during oxidation. It should be noted that these pretreatments of Ag-SPE are performed in order to obtain reproducible results that guarantee the extraction of representative conclusions.

RESULTS AND DISCUSSION

EC-SOERS of different molecules

As was aforementioned, EC-SOERS was first reported in acidic solutions in presence of specific concentrations of KCl, obtaining the best response for UA using 0.1 M $HClO_4$ + $5 \cdot 10^{-3}$ M KCl. However, the replacement of KCl by $5 \cdot 10^{-3}$ M KBr also provided good experimental results in an EC-SOERS experiment.

Figure 1 shows the spectroelectrochemical responses of different molecules tested using a solution containing 0.1 M $HClO_4$ + $5 \cdot 10^{-3}$ M KBr. For simplicity in the terminology, the representation of the evolution of the intensity of a Raman band at one specific Raman shift as a function of the applied potential will be denoted as voltaRamangram [23]. Figures 1A, 1B and 1C show the CV (orange curve) and the voltaRamangram (blue curve) obtained at a significant Raman shift of each molecule using a silver disk electrode, for BzA, sorbic acid

and caffeine, respectively. Whereas, Figures 1D, 1E and 1F show the CV and voltaRamangram obtained at a significant Raman shift of each molecule with Ag-SPEs, for salicylic acid, acetylsalicilic acid (AcSa) and citric acid, respectively.

Figure 1.

As can be observed, EC-SOERS is obtained in both Ag disk electrode and Ag-SPE for different molecules. All CVs (orange curves, Figure 1) have a similar behavior, displaying a first oxidation peak around +0.10 V that corresponds to the silver oxidation and the subsequent generation of AgBr. After this process, the silver electrode is massively oxidized to Ag^+ at potentials higher than +0.40 V, as was discussed in a previous work [23] (see Figure S1 for more detail). At this oxidation stage, the intensity of a characteristic Raman band of each molecule increases due to the EC-SOERS effect, as can be seen in the voltaRamangrams (blue curves, Figure 1). The spectrum of each molecule at the positive vertex potential, +0.55 V, can be observed in Figure S2, being unequivocally ascribed to the corresponding studied molecule (Table S1).

Reversing the scan, the reduction of the oxidized silver species is observed in the CVs with a cathodic peak centered around +0.35 V, which, in some cases, is accompanied by a mild increase in the Raman intensity for the molecule studied in the voltaRamangrams (Figures 1A, 1B, 1E and 1F). Interestingly, after this electrochemical reduction process, the Raman intensity falls to zero in most of the studied molecules. Finally, a second reduction process is observed at around –0.10 V, related to the reduction of AgBr to Ag [34]. It is remarkable that a two-step reduction process is clearly observed in the CV recorded using the Ag disk electrode when the reduction of AgBr takes place (orange curves in Figures 1A, 1B and 1C).

Conversely, only one broad voltammetric peak evolves at Ag-SPEs. Finally, it should be noted that after the last reduction process, only two molecules (sorbic acid and caffeine, blue curves in Figures 1B and 1C) shows a very small Raman enhancement in the cathodic region (below 0 V) due to SERS effect.

This behavior indicates that these two molecules are active both in EC-SERS and EC-SOERS, while the other molecules tested are only active in EC-SOERS under these experimental conditions. Thus, the differences described above between EC-SERS and EC-SOERS responses suggest that the two enhancements are related to different phenomena and its effect in the enhancement of the Raman signal is very different.

The waveform of the voltammograms is similar in all cases, but the shape of the voltaRamangrams (blue curves) clearly depends on the molecule. Consequently, it is inferred that the chemical interaction of each molecule with the electrode surface is highly responsible for this enhancement. From the results shown in Figure 1, it can be inferred that although EC-SOERS in KBr medium is observed for very different molecules, it is particularly intense for compounds that contain carbonyl or carboxylic groups, aromatic rings and/or π–delocalized systems.

In previous works, EC-SOERS phenomenon observed in KCl medium has been used for quantitative analysis [23,35]. Consequently, the relationship between the EC-SOERS signal observed in KBr medium for a specific molecule and its concentration has been also evaluated. Figure 2 shows the calibration curve of AcSa in a 0.1 M $HClO_4$ + $5 \cdot 10^{-3}$ M KBr solution. As can be seen, a good linear correlation is obtained (R^2=0.996) with low %RSD values. Therefore, EC-SOERS in KBr medium can be also used for quantitative analysis.

Figure 2.

Chemical selectivity of EC-SOERS

Although EC-SOERS can be observed in both KCl and KBr medium, the spectroscopic responses recorded in the two electrolytic media are not similar for the same analyte. Surprisingly, in the case of UA, the change of the halide (using KBr instead of KCl) leads to a decrease of the EC-SOERS signal (Figure S3A). Conversely, in the case of BzA, the change of KCl for KBr enhances drastically the EC-SOERS signal (Figure S3B). Therefore, the interaction of the target molecule with the structures responsible of the enhancement is fundamental to obtain the amplification of the Raman signal.

Previous studies related to EC-SOERS responses for UA revealed that not only KCl concentration, but also solution pH affects significantly to the Raman enhancement [33]. After an optimization process, it was stated that UA showed a poor EC-SOERS signal for pH values higher than 1 and KCl concentrations exceeding $1 \cdot 10^{-2}$ M. Herein, we will demonstrate that EC-SOERS signal for BzA is more intense in KBr medium, and it benefits from pH higher than 1 and halide concentrations higher than $1 \cdot 10^{-2}$ M.

With the aim of maximizing the EC-SOERS signal of BzA, we studied the effect of the electrolytic media in the spectroelectrochemical response. A two factor at three levels central composite experimental design was developed to optimize the values of KBr concentration and pH (Table S2). Figure S4 shows the EC-SOERS responses for each experiment, verifying their dependence on the KBr concentration and the pH value. It is noteworthy that the behavior of BzA is completely different than the one reported for UA in KCl [33]. The maximum EC-SOERS signal for BzA was observed at 0.05 M KBr and pH=2.9 (Figure

S4G) while for UA was $5 \cdot 10^{-3}$ M KCl and pH=1 [33]. These results demonstrate that EC-SOERS strongly depends on the studied molecule, the halide used and the pH of the solution.

The fact that EC-SOERS signals of UA and BzA show clear different behavior depending on the electrolyte (change of halide), could be used to obtain chemical selectivity by changing the halide used in the experiment. In this sense, Figure 3 compares the evolution of the voltaRamangram for UA and BzA in two different electrolytic media, 0.1 M $HClO_4$ + $5 \cdot 10^{-3}$ M KCl solution (pH=1, blue curve) and $1 \cdot 10^{-3}$ M $HClO_4$ + $5.4 \cdot 10^{-2}$ M $LiClO_4$ + $5 \cdot 10^{-2}$ M KBr solution (pH=2.9, orange curve), on a Ag-SPE substrate. Ag-SPEs were chosen instead of silver disk electrodes to ensure reproducibility of the spectroscopic measurements and to make easier to reproduce these SEC experiments for the scientific community. Nevertheless, the experiments have been also performed using silver disk electrodes with similar results.

Figure 3.

Figure 3A shows both the Raman spectra at three selective potentials (inset Figure 3A) and the voltaRamangram at 641 cm^{-1}, a characteristic Raman band of UA, in the two electrolytic media indicated above. At potentials lower than c.a. +0.40 V, no Raman signal is observed, as demonstrated in the full spectra (inset Figure 3A) and the voltaRamangram (blue curve, Figure 3A). However, at potentials from +0.40 V onwards, where massive oxidation of silver takes place (see CV, blue curve in Figure S5A), the typical Raman spectra for UA are observed (spectrum at +0.60 V in Figure 3A and Figure S6A). It is noteworthy that the enhancement of the Raman signal for UA can only be observed in the electrolytic medium with KCl (0.1 M $HClO_4$+ $5 \cdot 10^{-3}$ M KCl, pH=1). When the electrolytic medium with KBr

was used ($1 \cdot 10^{-3}$ M $HClO_4$ + $5.4 \cdot 10^{-2}$ M $LiClO_4$ + $5 \cdot 10^{-2}$ M KBr solution, pH = 2.9), no enhancement of the Raman signal was observed (orange curve, Figure 3A). This fact results extremely useful in situations where UA acts as interferent of other analytes, since it can be used to avoid the interference in analytical applications.

On the other hand, Figure 3B shows the progressive enhancement of the Raman signal for BzA as applied potential exceed +0.40 V (inset in Figure 3B and spectrum in Figure S6B), using the electrolytic medium containing KBr ($1 \cdot 10^{-3}$ M $HClO_4$ + $5.4 \cdot 10^{-2}$ M $LiClO_4$ + $5 \cdot 10^{-2}$ M KBr solution). In this case, Raman intensities for BzA reach values as high as $4 \cdot 10^4$ counts, even using 1 s of integration time. The analytical enhancement factor (AEF) [36] calculated with the former value of Raman intensity for BzA is approximately $2.5 \cdot 10^4$, an enhancement of two orders of magnitude greater than the observed using the electrolytic medium containing KCl (0.1 M $HClO_4$+ $5 \cdot 10^{-3}$ M KCl solution) [23].

This behavior evidences two important points for EC-SOERS: (1) AEF higher than 10^3 can be obtained, suggesting that not only the chemical effect is responsible of this enhancement. This mean that some kind of plasmonic nanostructure should be generated at anodic potentials, and it should be involved in the amplification of the Raman signal [4]. (2) EC-SOERS shows a very interesting chemical selectivity that can be achieved by the modulation of the electrolytic medium. In fact, this chemical selectivity has proved to be useful to resolve mixtures of the studied analytes, as demonstered in Figure S7, where only the band corresponding to BzA increases during the oxidation of the silver electrode in a KBr medium, while no bands related to UA are observed.

SEM study of the electrode during an EC-SOERS experiments

In an attempt to shed more light on the origin of the EC-SOERS phenomenon, the morphology of the electrode surface was studied by field emission scanning electronic microscopy (FE-SEM). Different samples were prepared during Raman-SEC experiments to observe the influence of the electrolytic medium on the modification of the electrode surface after different treatments. Figure 4 shows FE-SEM images of different Ag-SPE substrates after applying LSV scans from 0.00 V to +0.60 V in the two electrolytic media, 0.1 M $HClO_4$ + $5 \cdot 10^{-3}$ M KCl and $1 \cdot 10^{-3}$ M $HClO_4$ + $5.4 \cdot 10^{-2}$ M $LiClO_4$ + $5 \cdot 10^{-2}$ M KBr.

Figure 4A shows the FE-SEM image of the final surface for the Ag-SPE after stopping the potential scan at +0.60 V, conditions where the highest EC-SOERS enhancement was found for BzA ($1 \cdot 10^{-3}$ M $HClO_4$ + $5.4 \cdot 10^{-2}$ M $LiClO_4$ + $5 \cdot 10^{-2}$ M KBr solution). Under these conditions, rock-like structures of AgBr are formed during the silver oxidation, as evidences SEM image (Figure 4A) and EDX analysis (Figure S8). The formation of these structures leads to a noticeable increment of the surface area, in agreement with other results found in literature [37], due to the roughening of the electrode surface. These results contrast with the cubic structures observed after a similar experiment in presence of UA in 0.1 M $HClO_4$ + $5 \cdot 10^{-3}$ M KCl solution, as is shown in Figure 4B. In this case, cubic-shaped particles of AgCl are formed during the oxidation of the electrode with a silver enrichment on the surface of such structures [23]. The differences between these two structures (cubes and rocks) formed during silver oxidation could be the origin of the detected chemical selectivity of the phenomenon. Some works have reported an increment of the Raman signal for pyridine and other molecules adsorbed on Ag^+/AgCl or Ag/AgCl structures [38–41]. However, our structures do not enhance the Raman response of pyridine or cyanide. Moreover, the role of

the applied potential is fundamental in the generation of the Raman enhancement, as will be shown in the next section. Therefore, the surface structures by themselves cannot easily explain the origin of the enhancement. As a conclusion, these FE-SEM images evidences that silver halide microstructures were generated on the electrode surface during EC-SOERS, but at this point we can not confirm if those structures are directly responsible of the phenomenon.

Figure 4.

Effect of the potential on the enhancement of Raman signals by EC-SOERS

In previous works, we demonstrated that EC-SOERS in KCl is an intrinsically electrochemical process, the application of oxidation potentials is mandatory to observe the phenomenon [23]. This important fact has been also corroborated for BzA in KBr medium by using chronoamperometry (CA) to generate the Raman enhancement. Figure 5 displays the chronoRamangram (evolution of the Raman intensity at a specific Raman shift during a CA experiment) of the main band of BzA (1005 cm^{-1}) during a multistep CA experiment, compared with the corresponding current intensity. CA protocol was carried out in a $1 \cdot 10^{-3}$ M $HClO_4$ + $5.4 \cdot 10^{-2}$ M $LiClO_4$ + $5 \cdot 10^{-2}$ M KBr solution. It consisted of a first anodic pulse at +0.60 V for 15 s, followed by a second pulse at open circuit potential (OCP) for 15 s, and finally, a cathodic pulse at -0.40 V for 20 s. As can be observed, the enhancement strongly depends on the applied potential, as it was previously demonstrated for UA in a 0.1 M $HClO_4$ + $5 \cdot 10^{-3}$ M KCl solution [23]. The Raman enhancement related to BzA is only observed during the oxidation of the Ag electrode at +0.60 V and the signal disappears when the system is left at OCP. It is noteworthy that no signal is observed at -0.40 V, conditions at

which the reduction of the oxidized silver species is favored. This fact points out that both, the electrochemical potential and the formation of some kind of nanostructures on the electrode surface during the substrate oxidation play a key role for the enhancement of the Raman signal.

Figure 5.

From the TR-Raman-SEC experiments and from the FE-SEM images we can deduce that silver halides nanostructures are not the main responsible structure that enhances the Raman signal, which is reasonable since silver halides alone are not expected to have plasmonic properties. It is true that Ag@AgBr structures have been used for plasmonic photocatalysis [42], but the necessity of having potentials higher than +0.40 V makes difficult to think that Ag@AgBr species are the responsible of EC-SOERS, as this potential is enough to massively oxidize the substrate.

Nevertheless, electrolytic media containing halides clearly help to increase the enhancement of the Raman signal, playing a fundamental role in the EC-SOERS effect for specific molecules. Moreover, such Raman enhancement can only be observed during the application of a possitive potential, and it vanishes at OCP conditions. Therefore, i*n-situ* and *operando* techniques should be used to shed more light on this intriguing phenomenon. Nevertheless, the possibility of using EC-SOERS phenomenon at conditions at which chemical selectivity could be achieved has been demonstrated.

CONCLUSIONS

To summarize, EC-SOERS has been observed in KBr medium for the first time. It has been also proved that EC-SOERS can provide chemical selectivity by tailoring of the electrolytic medium, where pH and precipitant agent (KCl or KBr) and its concentration play a fundamental role. The different electrolytic media promote the generation of diverse silver halide structures on the electrode surface during silver oxidation process. In this sense, the origin of the observed enhancement should involve some kind of electromagnetic effect since it shows analytical enhancement factors higher than 10^4, one order of magnitude higher to the maximum enhancement usually attributed to the chemical mechanism [3,4,43]. EC-SOERS has been observed for different kind of molecules, especially those molecules containing carboxylic acids and aromatic rings with carbonyl groups. Interestingly, EC-SOERS has not been still observed in positive charged molecules, unless they contain carbonyl or carboxyl groups. The results obtained in KBr medium are very different compared to the ones obtained in KCl medium, yielding very different structures during the oxidation of the electrode surface. The specific interaction of these structures with the target molecule remains unknown. Therefore, further *in-situ* and *operando* studies must be carried out to understand this new and promising phenomenon that cannot be easily explained using the existing models.

ACKNOWLEDGEMENTS

Authors acknowledge the financial support from Ministerio de Economía y Competitividad (Grants CTQ2017-83935-R-AEI/FEDERUE), Junta de Castilla y León (BU297P18) and Ministerio de Ciencia, Innovación y Universidades (RED2018-102412-T). J.V.P-R. thanks JCyL for his postdoctoral fellowship (Grant BU033-U16). S.H. thanks JCyL and European Social Fund for her predoctoral fellowship and M.P-E. thanks its contract funded by JCyL, the European Social Fund and the Youth Employment Initiative.

REFERENCES

[1] J. Langer, D. Jimenez de Aberasturi, J. Aizpurua, R.A. Alvarez-Puebla, B. Auguié, J.J. Baumberg, G.C. Bazan, S.E.J. Bell, A. Boisen, A.G. Brolo, J. Choo, D. Cialla-May, V. Deckert, L. Fabris, K. Faulds, F.J. García de Abajo, R. Goodacre, D. Graham, A.J. Haes, C.L. Haynes, C. Huck, T. Itoh, M. Käll, J. Kneipp, N.A. Kotov, H. Kuang, E.C. Le Ru, H.K. Lee, J.-F. Li, X.Y. Ling, S.A. Maier, T. Mayerhöfer, M. Moskovits, K. Murakoshi, J.-M. Nam, S. Nie, Y. Ozaki, I. Pastoriza-Santos, J. Perez-Juste, J. Popp, A. Pucci, S. Reich, B. Ren, G.C. Schatz, T. Shegai, S. Schlücker, L.-L. Tay, K.G. Thomas, Z.-Q. Tian, R.P. Van Duyne, T. Vo-Dinh, Y. Wang, K.A. Willets, C. Xu, H. Xu, Y. Xu, Y.S. Yamamoto, B. Zhao, L.M. Liz-Marzán, Present and Future of Surface-Enhanced Raman Scattering, ACS Nano. 14 (2020) 28–117. https://doi.org/10.1021/acsnano.9b04224.

[2] P.L. Stiles, J.A. Dieringer, N.C. Shah, R.P. Van Duyne, Surface-Enhanced Raman Spectroscopy, Annu. Rev. Anal. Chem. 1 (2008) 601–626. https://doi.org/10.1146/annurev.anchem.1.031207.112814.

[3] M. Fleischmann, P.J. Hendra, A.J. McQuillan, Raman spectra of pyridine adsorbed at a silver electrode, Chem. Phys. Lett. 26 (1974) 163–166. https://doi.org/10.1016/0009-2614(74)85388-1.

[4] B. Sharma, R.R. Frontiera, A.-I. Henry, E. Ringe, R.P. Van Duyne, SERS: Materials, applications, and the future, Mater. Today. 15 (2012) 16–25. https://doi.org/10.1016/S1369-7021(12)70017-2.

[5] S.-Y. Ding, E.-M. You, Z.-Q. Tian, M. Moskovits, Electromagnetic theories of surface-

enhanced Raman spectroscopy, Chem. Soc. Rev. 46 (2017) 4042–4076. https://doi.org/10.1039/C7CS00238F.

[6] M. Musiani, J.-Y. Liu, Z.-Q. Tian, Applications of Electrochemical Surface-Enhanced Raman Spectroscopy (EC-SERS), in: Z.-Q.T. and D.E.W. Derek Pletcher (Ed.), Dev. Electrochem., First, John Wiley & Sons, Ltd, Chichester, UK, 2014: pp. 137–162. https://doi.org/10.1002/9781118694404.ch8.

[7] Z. Tian, X.-M. Zhang, Electrochemical Surface-Enhanced Raman Spectroscopy (EC-SERS): Early History, Principles, Methods, and Experiments, in: Dev. Electrochem., John Wiley & Sons, Ltd, Chichester, UK, 2014: pp. 113–135. https://doi.org/10.1002/9781118694404.ch7.

[8] R.A. Alvarez-Puebla, L.M. Liz-Marzán, SERS Detection of Small Inorganic Molecules and Ions, Angew. Chemie Int. Ed. 51 (2012) 11214–11223. https://doi.org/10.1002/anie.201204438.

[9] X. Wang, W. Shi, Z. Jin, W. Huang, J. Lin, G. Ma, S. Li, L. Guo, Remarkable SERS Activity Observed from Amorphous ZnO Nanocages, Angew. Chemie Int. Ed. 56 (2017) 9851–9855. https://doi.org/10.1002/anie.201705187.

[10] K.W. Kho, C.Y. Fu, U.S. Dinish, M. Olivo, Clinical SERS: are we there yet?, J. Biophotonics. 4 (2011) 667–684. https://doi.org/10.1002/jbio.201100047.

[11] C.-Y. Li, S.-Y. Chen, Y.-L. Zheng, S.-P. Chen, R. Panneerselvam, S. Chen, Q.-C. Xu, Y.-X. Chen, Z.-L. Yang, D.-Y. Wu, J.-F. Li, Z.-Q. Tian, In-situ electrochemical shell-isolated Ag nanoparticles-enhanced Raman spectroscopy study of adenine adsorption on

smooth Ag electrodes, Electrochim. Acta. 199 (2016) 388–393. https://doi.org/10.1016/j.electacta.2016.03.065.

[12] K. Kneipp, H. Kneipp, I. Itzkan, R.R. Dasari, M.S. Feld, Surface-enhanced Raman scattering and biophysics, J. Phys. Condens. Matter. 14 (2002) 202. https://doi.org/10.1088/0953-8984/14/18/202.

[13] J.F. Li, Y.F. Huang, Y. Ding, Z.L. Yang, S.B. Li, X.S. Zhou, F.R. Fan, W. Zhang, Z.Y. Zhou, D.Y. Wu, B. Ren, Z.L. Wang, Z.Q. Tian, Shell-isolated nanoparticle-enhanced Raman spectroscopy, Nature. 464 (2010) 392–395. https://doi.org/10.1038/nature08907.

[14] Z.-C. Zeng, S. Hu, S.-C. Huang, Y.-J. Zhang, W.-X. Zhao, J.-F. Li, C. Jiang, B. Ren, Novel Electrochemical Raman Spectroscopy Enabled by Water Immersion Objective, Anal. Chem. 88 (2016) 9381–9385. https://doi.org/10.1021/acs.analchem.6b02739.

[15] G. Sharma, T. Deckert-Gaudig, V. Deckert, Tip-enhanced Raman scattering-Targeting structure-specific surface characterization for biomedical samples, Adv. Drug Deliv. Rev. 89 (2015) 42–56. https://doi.org/10.1016/j.addr.2015.06.007.

[16] L. Cui, D. Zhang, K. Yang, X. Zhang, Y.-G. Zhu, Perspective on Surface-Enhanced Raman Spectroscopic Investigation of Microbial World, Anal. Chem. 91 (2019) 15345–15354. https://doi.org/10.1021/acs.analchem.9b03996.

[17] Z.-Q. Tian, B. Ren, D.-Y. Wu, Surface-Enhanced Raman Scattering: From Noble to Transition Metals and from Rough Surfaces to Ordered Nanostructures, J. Phys. Chem. B. 106 (2002) 9463–9483. https://doi.org/10.1021/jp0257449.

[18] Y.-F. Huang, H.-P. Zhu, G.-K. Liu, D.-Y. Wu, B. Ren, Z.-Q. Tian, When the Signal Is

Not from the Original Molecule To Be Detected: Chemical Transformation of para - Aminothiophenol on Ag during the SERS Measurement, J. Am. Chem. Soc. 132 (2010) 9244–9246. https://doi.org/10.1021/ja101107z.

[19] A.M. Robinson, S.G. Harroun, J. Bergman, C.L. Brosseau, Portable Electrochemical Surface-Enhanced Raman Spectroscopy System for Routine Spectroelectrochemical Analysis, Anal. Chem. 84 (2012) 1760–1764. https://doi.org/10.1021/ac2030078.

[20] C. Zong, C.-J. Chen, M. Zhang, D.-Y. Wu, B. Ren, Transient Electrochemical Surface-Enhanced Raman Spectroscopy: A Millisecond Time-Resolved Study of an Electrochemical Redox Process, J. Am. Chem. Soc. 137 (2015) 11768–11774. https://doi.org/10.1021/jacs.5b07197.

[21] J. Wang, X. Mu, M. Sun, Optical-electrical synergy on electricity manipulating plasmon-driven photoelectrical catalysis, Appl. Mater. Today. 15 (2019) 305–314. https://doi.org/10.1016/j.apmt.2019.02.011.

[22] T.P. Lynk, C.S. Sit, C.L. Brosseau, Electrochemical Surface-Enhanced Raman Spectroscopy as a Platform for Bacterial Detection and Identification, Anal. Chem. 90 (2018) 12639–12646. https://doi.org/10.1021/acs.analchem.8b02806.

[23] J. V. Perales-Rondon, S. Hernandez, D. Martin-Yerga, P. Fanjul-Bolado, A. Heras, A. Colina, Electrochemical surface oxidation enhanced Raman scattering, Electrochim. Acta. 282 (2018) 377–383. https://doi.org/10.1016/j.electacta.2018.06.079.

[24] S.-Y. Ding, E.-M. You, Z.-Q. Tian, M. Moskovits, Electromagnetic theories of surface-enhanced Raman spectroscopy, Chem. Soc. Rev. 46 (2017) 4042–4076.

https://doi.org/10.1039/C7CS00238F.

[25] D.-Y. Wu, J.-F. Li, B. Ren, Z.-Q. Tian, Electrochemical surface-enhanced Raman spectroscopy of nanostructures, Chem. Soc. Rev. 37 (2008) 1025. https://doi.org/10.1039/b707872m.

[26] B. Huang, H. Yang, L. Zhang, Y. Yuan, Y. Cui, J. Zhang, Effect of surface/interfacial defects on photo-stability of thick-shell CdZnSeS/ZnS quantum dots, Nanoscale. 10 (2018) 18331–18340. https://doi.org/10.1039/C8NR04224A.

[27] P. Gao, D. Gosztola, L.-W.H. Leung, M.J. Weaver, Surface-enhanced Raman scattering at gold electrodes: dependence on electrochemical pretreatment conditions and comparisons with silver, J. Electroanal. Chem. Interfacial Electrochem. 233 (1987) 211–222. https://doi.org/10.1016/0022-0728(87)85017-9.

[28] Y.-C. Liu, C.-C. Wang, C.-E. Tsai, Effects of electrolytes used in roughening gold substrates by oxidation–reduction cycles on surface-enhanced Raman scattering, Electrochem. Commun. 7 (2005) 1345–1350. https://doi.org/10.1016/j.elecom.2005.09.030.

[29] A. Kudelski, J. Bukowska, M. Janik-Czachor, W. Grochala, A. Szummer, M. Dolata, Characterization of the copper surface optimized for use as a substrate for surface-enhanced Raman scattering, Vib. Spectrosc. 16 (1998) 21–29. https://doi.org/10.1016/S0924-2031(97)00049-0.

[30] Q. Gao, A. Zhao, Z. Gan, W. Tao, D. Li, M. Zhang, H. Guo, D. Wang, H. Sun, R. Mao, E. Liu, Facile fabrication and growth mechanism of 3D flower-like Fe3O4

nanostructures and their application as SERS substrates, CrystEngComm. 14 (2012) 4834–4842. https://doi.org/10.1039/C2CE25198A.

[31] E.C. Le Ru, J. Grand, N. Félidj, J. Aubard, G. Lévi, A. Hohenau, J.R. Krenn, E. Blackie, P.G. Etchegoin, Experimental Verification of the SERS Electromagnetic Model beyond the | E | 4 Approximation: Polarization Effects, J. Phys. Chem. C. 112 (2008) 8117–8121. https://doi.org/10.1021/jp802219c.

[32] E. V. Formo, S.M. Mahurin, S. Dai, Robust SERS Substrates Generated by Coupling a Bottom-Up Approach and Atomic Layer Deposition, ACS Appl. Mater. Interfaces. 2 (2010) 1987–1991. https://doi.org/10.1021/am100272h.

[33] J. V. Perales-Rondon, S. Hernandez, A. Heras, A. Colina, Effect of chloride and pH on the electrochemical surface oxidation enhanced Raman scattering, Appl. Surf. Sci. 473 (2019) 366–372. https://doi.org/10.1016/j.apsusc.2018.12.148.

[34] T. Shimooka, J. Inukai, K. Itaya, Adlayer Structures of Cl and Br and Growth of Bulk AgBr Layers on Ag(100) Electrodes, J. Electrochem. Soc. 149 (2002) E19. https://doi.org/10.1149/1.1431965.

[35] S. Hernandez, J. V. Perales-Rondon, A. Heras, A. Colina, Determination of uric acid in synthetic urine by using electrochemical surface oxidation enhanced Raman scattering, Anal. Chim. Acta. 1085 (2019) 61–67. https://doi.org/10.1016/j.aca.2019.07.057.

[36] E.C. Le Ru, E. Blackie, M. Meyer, P.G. Etchegoin, Surface Enhanced Raman Scattering Enhancement Factors: A Comprehensive Study, J. Phys. Chem. C. 111 (2007) 13794–13803. https://doi.org/10.1021/jp0687908.

[37] W. Wang, Y. Huang, D. Liu, F. Wang, Z. Tian, D. Zhan, Electrochemically roughened gold microelectrode for surface-enhanced Raman spectroscopy, J. Electroanal. Chem. 779 (2016) 126–130. https://doi.org/10.1016/j.jelechem.2016.04.008.

[38] Y.-F. Cheng, Q. Cao, J. Zhang, T. Wu, R. Che, Efficient photodegradation of dye pollutants using a novel plasmonic AgCl microrods array and photo-optimized surface-enhanced Raman scattering, Appl. Catal. B Environ. 217 (2017) 37–47. https://doi.org/10.1016/j.apcatb.2017.05.021.

[39] Z. Gan, A. Zhao, M. Zhang, D. Wang, W. Tao, H. Guo, D. Li, M. Li, Q. Gao, A facile strategy for obtaining fresh Ag as SERS active substrates, J. Colloid Interface Sci. 366 (2012) 23–27. https://doi.org/10.1016/j.jcis.2011.09.052.

[40] N. Zhao, X. Fei, X. Cheng, J. Yang, Synthesis of silver/silver chloride/graphene oxide composite and its surface-enhanced Raman scattering activity and self-cleaning property, IOP Conf. Ser. Mater. Sci. Eng. 242 (2017) 012002. https://doi.org/10.1088/1757-899X/242/1/012002.

[41] L. Dawei, W. Jian, X. Houwen, S. Xu, L. Fan-chen, Enhancement origin of SERS from pyridine adsorbed on AgCl colloids, Spectrochim. Acta Part A Mol. Spectrosc. 43 (1987) 379–382. https://doi.org/10.1016/0584-8539(87)80120-4.

[42] P. Wang, B. Huang, X. Zhang, X. Qin, H. Jin, Y. Dai, Z. Wang, J. Wei, J. Zhan, S. Wang, J. Wang, M.-H. Whangbo, Highly Efficient Visible-Light Plasmonic Photocatalyst Ag@AgBr, Chem. - A Eur. J. 15 (2009) 1821–1824. https://doi.org/10.1002/chem.200802327.

[43] S. Zhang, W. Ma, F. Zhang, C. Jing, R. Wu, Theoretical and experimental study on adsorption of benzoic acid molecules on silver clusters, Ferroelectrics. 528 (2018) 99–107. https://doi.org/10.1080/00150193.2018.1448624.

Figure captions

Figure 1. VoltaRamangrams (blue curves) and CVs (orange curve) from $5 \cdot 10^{-3}$ M BzA (A), $2.4 \cdot 10^{-3}$ M sorbic acid (B), $5 \cdot 10^{-3}$ M caffeine (C), $1.5 \cdot 10^{-3}$ M salicylic acid (D), $1 \cdot 10^{-3}$ M AcSa (E) and $5 \cdot 10^{-3}$ M citric acid (F) in 0.1 M $HClO_4$ + $5 \cdot 10^{-3}$ M KBr solutions. Substrate: silver disk electrode (A, B and C), and Ag-SPEs (D, E and F). Laser power was set to 80 mW. Integration time was 1 s.

Figure 2. Linear regression curve for AcSa using EC-SOERS signal during a TR-Raman-SEC experiment on Ag-SPEs. All measurements were carried out using freshly conditioned Ag-SPEs. Standard solutions: AcSa x M + 0.1 M $HClO_4$ + $5 \cdot 10^{-3}$ M KBr. Three replicates were measured for each sample. Laser conditions and integration times were the same used in Figure 1.

Figure 3. Raman spectra (inset) at selected potentials and voltaRamangrams at the most significant Raman bands of $2 \cdot 10^{-4}$ M UA (A) and $1 \cdot 10^{-3}$ M BzA (B) during LSVs performed between 0.00 V and +0.60 V at 0.02 $V \cdot s^{-1}$ using a Ag-SPE. Blue curves represent recorded results from 0.1 M $HClO_4$ + $5 \cdot 10^{-3}$ M KCl solution, orange curves are those from $1 \cdot 10^{-3}$ M $HClO_4$ + $5.4 \cdot 10^{-2}$ M $LiClO_4$ + $5 \cdot 10^{-2}$ M KBr. Integration time was 1 s. Laser conditions were the same used in Figure 1.

Figure 4. SEM images of an Ag-SPE treated by different Raman-SEC experiments: LSV from 0.00 V to +0.60 V at 0.02 $V \cdot s^{-1}$, stopping at +0.60 V (A), LSV from +0.20 V to +0.60 V stopping at +0.60 V (B). Experiment (A) was carried out in $1 \cdot 10^{-3}$ M $HClO_4$ + $5.4 \cdot 10^{-2}$ M $LiClO_4$ + $5 \cdot 10^{-2}$ M KBr + $1 \cdot 10^{-3}$ M BzA, whereas experiment (B) was carried out in 0.1 M $HClO_4$ + $5 \cdot 10^{-3}$ M KCl + $2 \cdot 10^{-4}$ M UA. Scan rate: 0.02 $V \cdot s^{-1}$.

Figure 5. (a) ChronoRamangram at 1005 cm-1 (blue curve) and (b) chronoamperogram (orange curve) during a multistep chronoamperometric experiment of $1 \cdot 10^{-3}$ M BzA in $1 \cdot 10^{-3}$ M $HClO_4$ + $5.4 \cdot 10^{-2}$ M $LiClO_4$ + $5 \cdot 10^{-2}$ M KBr solution using a Ag-SPE. Potential program: +0.60 V for 15 s, followed by an OCP for 15 s, finalizing with -0.40 V for 20 s. Laser conditions and integration times were the same used in Figure 1.

Figures

Figure 1.

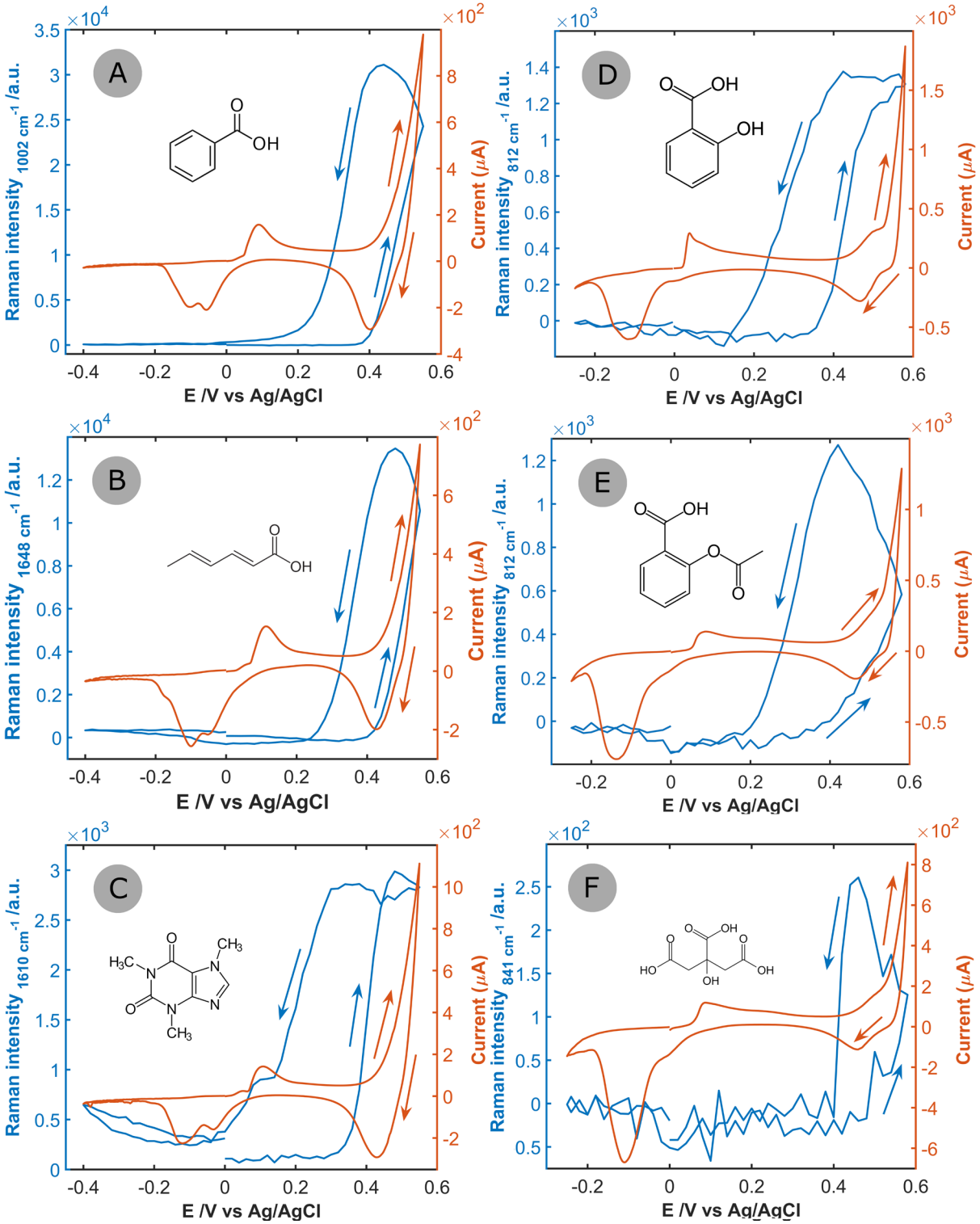

Figure 2.

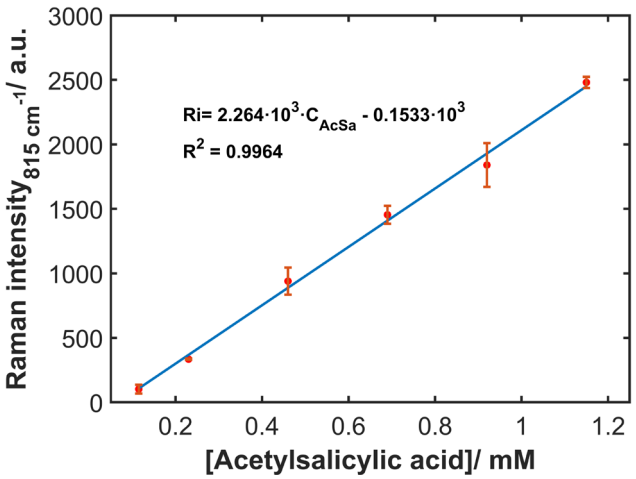
Raman intensity$_{815\ cm^{-1}}$/ a.u.
3000
2500
2000
1500
1000
500
0
0.2
0.4
0.6
0.8
1
1.2
[Acetylsalicylic acid]/ mM
Ri= 2.264·10^3·C$_{AcSa}$ - 0.1533·10^3
R^2 = 0.9964

Figure 3.

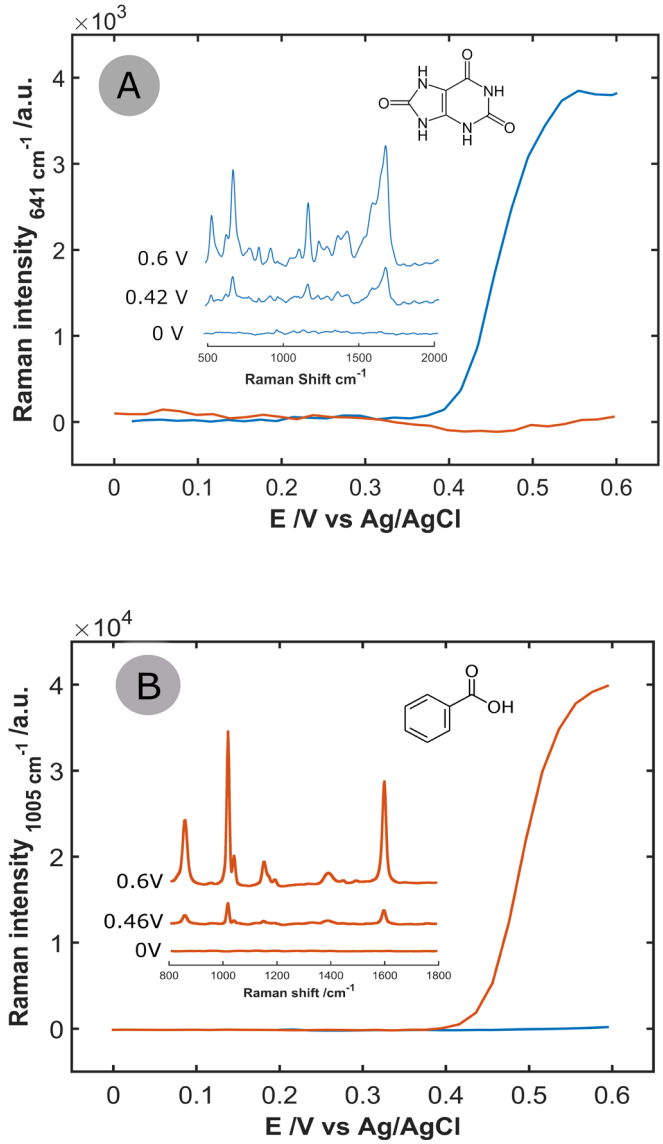
A
×10^3
Raman intensity 641 cm^-1 /a.u.
0.6 V
0.42 V
0 V
Raman Shift cm^-1
E /V vs Ag/AgCl
B
×10^4
Raman intensity 1005 cm^-1 /a.u.
0.6V
0.46V
0V
Raman shift /cm^-1
E /V vs Ag/AgCl

Figure 4.

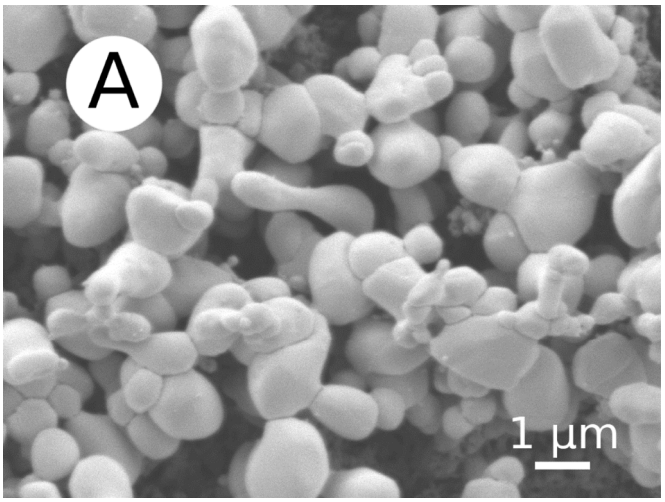

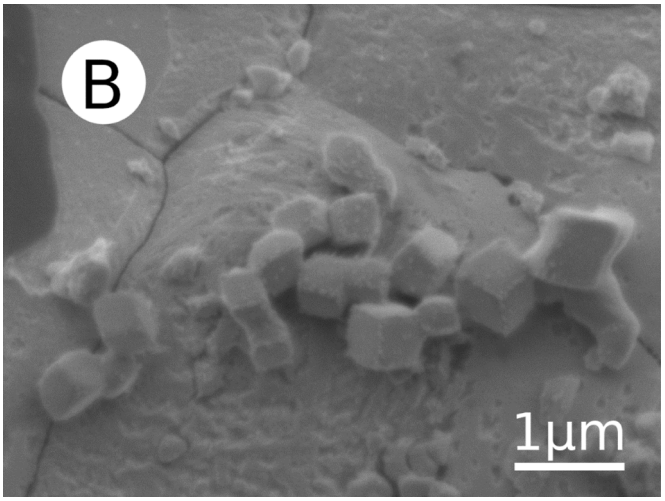

Figure 5.

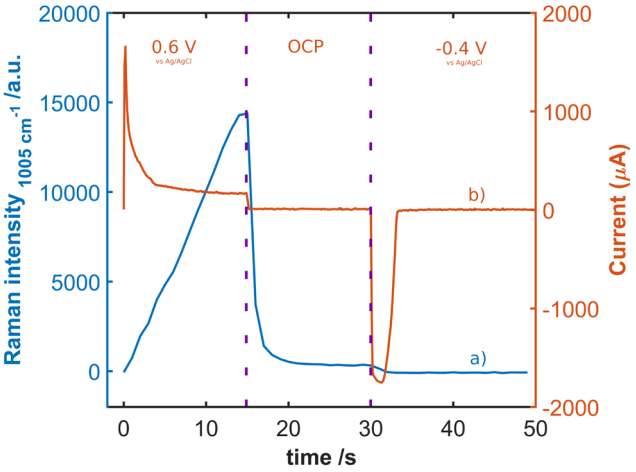
20000
15000
10000
5000
0
2000
1000
0
-1000
-2000
0.6 V
vs Ag/AgCl
OCP
-0.4 V
vs Ag/AgCl
b)
a)
0
10
20
30
40
50
time /s
Raman intensity 1005 cm-1 /a.u.
Current (μA)

Graphical Abstract